Journal of Luminescence 224 (2020) 117243

Contents lists available at ScienceDirect

Journal of Luminescence

journal homepage: http://www.elsevier.com/locate/jlumin

The effect of Gd^{3+} doping on luminescence properties of (Gd, Ce): SrF_2 nanopowders and transparent ceramics

Iva Milisavljevic [a], Yiquan Wu [a,**], Eugeniusz Zych [b]

[a] Kazuo Inamori School of Engineering, New York State College of Ceramics, Alfred University, Alfred, NY 14802, USA
[b] Faculty of Chemistry, University of Wroclaw, Wroclaw, 50-383, Poland

ARTICLE INFO

Keywords:
Transparent ceramics
UV emission
Radiative energy transfer

ABSTRACT

The effect of doping of Gd^{3+} ions into Ce: SrF_2 on luminescence properties was investigated in (Gd, Ce): SrF_2 nanoparticle powders synthesized via the co-precipitation method, which contained fixed amount of Ce^{3+} ions and variable amounts of Gd^{3+} ions. (Gd, Ce): SrF_2 nanoparticle powders showed UV range emissions under $\lambda_{ex} =$ 273 nm and $\lambda_{ex} =$ 298 nm excitation. Photoluminescence emission, excitation, and lifetime measurements revealed the existence of $Ce^{3+} \rightarrow Gd^{3+}$ radiative energy transfer and provided evidence to the prevailing effect of Ce^{3+} in excitation and emission in the (Gd, Ce) co-doped system due to the existence of fully allowed 4f-5d transitions. The presence of Gd^{3+} was shown to affect the crystal field and symmetry around Ce^{3+} ions and enhances the absorption efficiency by two-fold. Furthermore, (Gd, Ce): SrF_2 transparent ceramics with 13.2% of in-line optical transmittance in the UV spectral range was obtained via the vacuum hot-pressing method. The increase in the UV luminescence emission intensity of Ce^{3+} in presence of Gd^{3+}, as well as the ability to process (Gd, Ce): SrF_2 as transparent ceramics, are what make (Gd, Ce): SrF_2 a promising material for optical applications in the UV region.

1. Introduction

In the past decade, there has been considerable technological development of nanotechnologies and sintering techniques of ceramic materials which has led significant expansion in the field of transparent ceramics. Transparent ceramics have many advantages over single crystal materials such as simpler fabrication methods, lower costs of production, the possibility of fabricating large volumes and different structures, as well as production of materials which cannot be grown by conventional single crystal growth techniques [1]. Many authors have confirmed the potential use of transparent ceramics as optical and laser materials due to their properties [1,2]. Additionally, transparent ceramic materials can be homogeneously doped with laser-active ions such as rare-earth elements.

In terms of optical transparency and laser emission, most of the work done so far on transparent ceramics has been focused on emission in the visible and near infrared range of electromagnetic spectrum. Emission of blue, green, yellow or red light in various ceramic hosts has been discussed and is available in large quantities. However, there have been noticeably fewer reports on transparent ceramic materials with emission in the UV range, although UV emission has been observed in some systems.

Until now, the most promising UV emitting ceramic laser materials demonstrated have been oxide and fluoride ceramic materials. Qin *et al.* reported observation of UV upconversion luminescence in Ho^{3+}: Y_2O_3 [3] and (Ho, Gd): Y_2O_3 ceramics with co-doped Gd^{3+} and Ho^{3+} ions [4] under excitation of a 532 nm CW solid-state laser. On the other hand, Fujimoto *et al.* [5] observed UV luminescence in Yb^{3+}: $Y_3Al_5O_{12}$ (YAG) transparent ceramics due to the charge transfer between Yb^{3+} and O^{2-} under α-ray excitation. Yanagida *et al.* [6] reported photoluminescence (PL) emission in the UV range upon 280 nm excitation during their study on optical and scintillation properties of Yb^{3+}: Lu_2O_3 transparent ceramics. Furthermore, Nakamura *et al.* [7] reported emission peaks in the vacuum UV region in Nd^{3+}: CaF_2 transparent ceramic under 160 nm excitation which originated from the 5d-4f radiative transition in Nd^{3+}. Emission in the UV range was also observed in Ce^{3+}: BaF_2 [8] and Ce^{3+}: MgF_2 [9] transparent ceramics.

The unique optical properties of fluoride materials make them ideal candidates for various optical applications; these include lasers, windows, lenses and more, particularly in the UV and vacuum UV region [10]. Ce^{3+} ion has a $4f^1$ electronic configuration with 5d levels and is a widely used dopant which has high emission intensity due to the 5d-4f

* Corresponding author. Kazuo Inamori School of Engineering, New York State College of Ceramics, Alfred University, 2 Pine Street, Alfred, NY 14802, USA.
E-mail address: wuy@alfred.edu (Y. Wu).

https://doi.org/10.1016/j.jlumin.2020.117243
Received 3 May 2019; Received in revised form 1 March 2020; Accepted 25 March 2020
Available online 7 April 2020
0022-2313/© 2020 Elsevier B.V. All rights reserved.

transition, suitable for certain applications in which intense light emission is required [9]. UV emission of Ce^{3+}-doped alkaline-earth fluorides (MgF_2, CaF_2, SrF_2 and BaF_2) has been observed and studied in nanophosphors [11,12], crystals [13–15], and ceramics [8,9].

Furthermore, the co-doping effect of Ce^{3+} ions with Gd^{3+} ions has been studied in many different systems [16–24]. The Gd^{3+} ion itself exhibits UV emission, and it was found that the energy transfer from Gd^{3+} ions to other rare-earth ions can take place easily, except for Pr^{3+} and Tm^{3+} [24]. In many oxide and fluoride systems, the Gd^{3+} sublattice acts as a transportation system for the energy coming from the excitation source where both ^6I_J and ^6P_J energy states of Gd^{3+} can contribute to the energy transfer [23]. Additionally, energy transfer between Gd^{3+} and Ce^{3+} ions has been reported elsewhere [16,19,20,22], and it was even found to have a beneficial effect on Ce^{3+} luminescence emission in certain scenarios [18,21,24].

Current report investigates on the effects of co-doping of Gd^{3+} ions on luminescence properties of Ce: SrF_2 nanoparticles obtained by the co-precipitation method and discusses the nature of the energy transfer which occurs between Ce^{3+} and Gd^{3+} ions in this system. So far, there have been very few reports discussing the effects of co-doping of Gd^{3+} and Ce^{3+} ions in SrF_2 [25,26]. The synthesized nanoparticle powders were used later on for the fabrication of (Gd, Ce): SrF_2 transparent ceramics by the vacuum hot-pressing method (HP). The HP method has been proven to be a very efficient technique for obtaining high-quality transparent fluoride ceramics [27–29]. Furthermore, phase, microstructure and optical properties of the obtained ceramics are discussed in terms of potential optical application in the UV range.

2. Experimental

2.1. Sample preparation

The (Gd, Ce): SrF_2 nanoparticle powders were synthesized via the co-precipitation method at room temperature [27]. All the chemical reagents used were of analytical grade and did not require additional purification. The following commercially available products were used as chemical reagents: $Sr(NO_3)_2$ (≥99.0%, Sigma-Aldrich), $Gd(NO_3)_3{\cdot}6H_2O$ (99.9%, Sigma-Aldrich), $Ce(NO_3)_3{\cdot}6H_2O$ (99.99%, Alfa Aesar), KF (99% min., Alfa Aesar). Deionized water was used to synthesize and wash the particles. Six powder samples of empirical formula $Gd_xCe_ySr_{(1-x-y)}F_{2+x+y}$, were prepared following the composition ratio which included 3.0 at. % Ce^{3+} and different doping levels of Gd^{3+} (0.0, 0.5, 1.0, 1.5, 2.0, and 3.0 at. % Gd^{3+}). Additionally, a 0.5 at. % doped Gd: SrF_2 powder sample was prepared as a control sample for the optical absorption measurement. All the nitrate reagents were dissolved in water and mixed together using a magnetic stirrer. A KF aqueous solution was prepared separately in the same manner as the nitrate reagents, but with an appropriately excessive amount of KF. The KF aqueous solution was further added in a drop-wise manner to the nitrate solution under continuous stirring at 530 rpm for 10 min. As soon as the KF aqueous solution was added, a formation of white particles could be observed. The mixture of solutions was left for 12 h at room temperature. The powders were separated from the mother liquid by centrifugation at 7000 rpm for 30 min and then washed three times with deionized water in order to remove nitrates and possible impurities. Wet powder samples were dried in oven at 60 °C and crushed afterwards into a white powder using an agate mortar.

An as-prepared powder sample of (Gd, Ce): SrF_2 containing 1.5 at. % of Gd^{3+} and 3.0 at. % of Ce^{3+} was calcined in an argon gas atmosphere at 450 °C for 5 h prior to sintering. This step was performed in order to remove the nitrate residuals, which could not be removed by washing, and absorbed water molecules. Next, the powder sample was loaded into the graphite mold and sintered at 820 °C for 60 min in a vacuum hot-pressing furnace with a vacuum greater than 10^{-6} Pa and under a loading pressure of 30 MPa. To reveal the grain boundaries, the ceramic sample was polished and then thermally etched in an argon environment for 30 min at 500 °C.

2.2. Characterization

The phase of the as-synthesized nanoparticles and ceramics were identified via X-ray powder diffraction (XRD) (D5000, Siemens) using Cu *Kα* radiation (λ = 0.154056 nm) in the range of 20° to 80° 2θ. The diffractograms were used to calculate the crystallite size and lattice parameters. The morphology and the elemental analysis of the obtained nanoparticles were observed using field emission scanning electron microscope (FE-SEM) JEOL JSM-7800F, JEOL USA Inc. equipped with energy dispersive X-ray spectrometer (EDS) Octane Plus, AMETEK-EDAX. The microstructure of the ceramic samples was studied using scanning electron microscope (SEM) FEI Quanta 200F, Thermo Fisher Scientific. The average grain size of the obtained ceramics was calculated using the method of linear intercepts on at least 200 grains from SEM images and by multiplying the average measured linear intercept distance by a statistical factor of 1.56 [30]. Density of the sintered ceramics was measured by the Archimedes method using water as an immersion liquid. Photoluminescence excitation and emission spectra were obtained using a spectrofluorometer Fluorolog-3, HORIBA Jobin Yvon Inc. with a 450 W xenon lamp as a radiation source at room temperature. Fluorescence lifetime measurements were executed with an Edinburgh Instruments FLS-1000 spectrofluorometer at room temperature (RT) using picosecond pulsed LEDs, EPLED-270 emitting at 276.0 nm and EPLED-295 emitting at 299.7 nm, operated at either 0.2 MHz or 0.5 MHz repetition rate and emission bandwidth set at 6 nm or 8 nm. In-line optical transmittance of polished ceramic samples was measured over a wavelength range from 200 nm to 1000 nm using a UV–Visible spectrophotometer Evolution 220, Thermo Scientific. The same spectrophotometer was used for recording the absorption spectrum of a powder sample in the reflectance mode in the 250–500 nm range.

3. Results and discussion

3.1. (Gd, Ce): SrF_2 nanoparticles

In Fig. 1(a), XRD patterns are presented of the as-prepared nanoparticle powder samples of (Gd, Ce): SrF_2 which contain 3.0 at. % of Ce^{3+} ions and variable amount of Gd^{3+} ions (0.0, 0.5, 1.0, 1.5, 2.0, and 3.0 at. %). It should be noted that all the diffraction peaks correspond to the face centered cubic phase of the strontium fluoride structure (SrF_2, space group: *Fm3m*), which agrees well with the JCPDS standard card (PDF#04-002-2192). No second phases can be observed. A slight shift of (111) peak to smaller 2θ angles, in comparison to the standard data, can be noted in all samples. Such results can be an indication of an increase of the lattice parameters due to doping with rare-earth ions [31,32]. This could be due to the charge compensation with F^- ions when the divalent Sr^{2+} ions are being replaced by the trivalent Gd^{3+} ions. With each Gd^{3+} ion doped into the SrF_2 structure there must be one additional F^- ion incorporated to compensate for the charge difference. These F^- ions will occupy interstitial positions which will in turn cause an electronic repulsion with the F^- ions lying on the lattice sites [28,31].

Obtained XRD diffractions were further used to calculate average crystallite size and lattice parameters. From the full width at half maximum (FWHM) of all the peaks in the XRD patterns, average crystallite size of powder samples was estimated using the Scherrer equation [33]. Calculated average crystallite sizes are presented in the table in Fig. 1(b). It can be observed that the average crystallite sizes of all the samples are very similar to one another. The lattice parameter was calculated using Bragg's formula and expression for *d*-spacing in cubic systems. The computed values of the lattice parameters (*a*) are presented in Fig. 1(b).

Elemental analysis via EDS of the as-prepared powder samples confirmed the presence of Sr, F, Ce, and Gd. This indicates that the Ce^{3+}

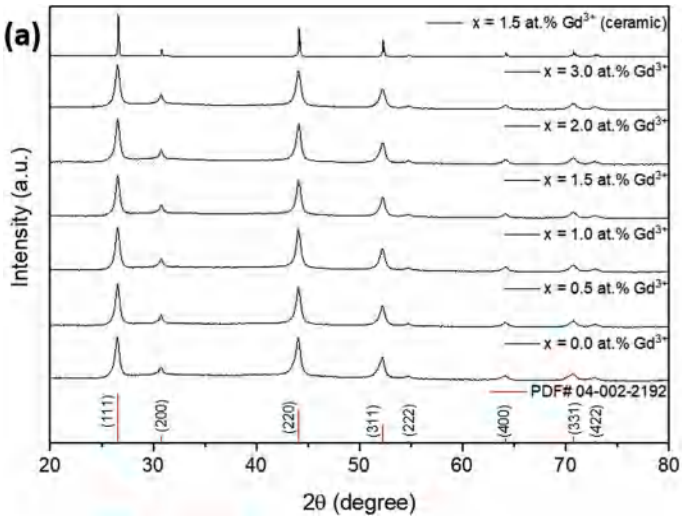

(b)

Sample ($x = Gd^{3+}$ at. %)	Lattice parameter, a (Å)	Average crystallite size, (nm)
x = 0.00	5.8211(6)	14.44
x = 0.50	5.8140(5)	15.86
x = 1.00	5.8142(7)	15.99
x = 1.50	5.8101(8)	15.96
x = 2.00	5.8114(7)	15.77
x = 3.00	5.8142(7)	15.05

Fig. 1. (a) XRD patterns of as-prepared 3.0 at. % Ce^{3+}: Gd_xSrF_2 (x = 0.0, 0.5, 1.0, 1.5, 2.0, and 3.0 at. % Gd^{3+}) powder samples and (Gd, Ce): SrF_2 (1.5 at. % Gd^{3+}, 3.0 at. % Ce^{3+}) transparent ceramics; (b) Calculated lattice parameter and average crystallite size.

and Gd^{3+} doping ions were successfully incorporated into the SrF_2 host lattice. Potassium (K) in amounts of 0.17–0.36 at. % was also identified in all of the powder samples. The K^+ ions originate from the KF that was used as a chemical reagent in the co-precipitation process. In Fig. 2(a), the calculated and measured values of Gd^{3+} and Ce^{3+} ions (in at. %) in each sample analyzed by EDS are graphically presented. It can be observed that there is a difference between the two values for both doping ions. In addition to the charge compensation with F^- ions

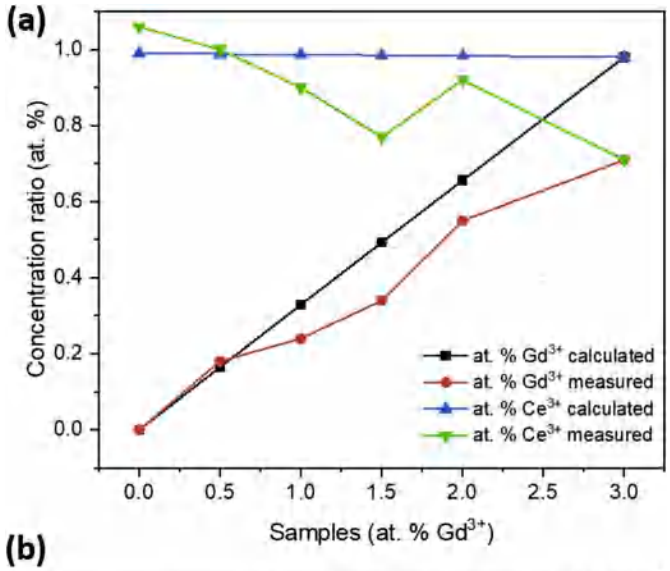

(b)

Sample ($x = Gd^{3+}$ at. %)	Measured concentration ratio (at. %)		
	Sr^{2+}	Ce^{3+}	Gd^{3+}
x = 0.00	28.96	1.06	0.00
x = 0.50	27.55	1.00	0.18
x = 1.00	26.60	0.90	0.24
x = 1.50	22.27	0.77	0.34
x = 2.00	25.96	0.92	0.55
x = 3.00	22.42	0.71	0.71

Fig. 2. (a) Graphical presentation of calculated values of Gd^{3+} and Ce^{3+} concentrations and values measured using EDS in powder samples, and (b) measured concentration ratios of Sr^{2+}, Ce^{3+}, and Gd^{3+} ions in 3.0 at. % Ce^{3+}: Gd_xSrF_2 as-prepared powder samples.

previously described, the charge imbalance resulted from doping with trivalent Gd^{3+} and Ce^{3+} ions could also be partially compensated with the incorporation of monovalent K^+ ions into the crystal lattice. This explains the presence of K^+ ions in the EDS spectra and the difference between the calculated and measured values for the Gd^{3+} and Ce^{3+} ions. Fig. 2(b) presents semi-quantitative data of concentration ratios of Sr^{2+}, Ce^{3+}, and Gd^{3+} ions in different powder samples calculated based on the EDS spectra. The obtained Sr: Ce: Gd ratios in all the samples are in agreement with the theoretical values.

Fig. 3 shows FE-SEM micrographs of as-prepared (Gd, Ce): SrF_2 nanoparticle powder samples with different Gd^{3+} concentrations. It can be observed that the particles are nearly spherical and agglomerated, as observed elsewhere for such system, which is expected considering that no surfactants have been used during powder synthesis. Additionally, there could not be observed a change in particle shape with an increase in the Gd^{3+} concentration.

Fig. 4 presents the RT photoluminescence emission and excitation spectra of the as-prepared (Gd, Ce): SrF_2 nanopowders, containing 3.0 at. % of Ce^{3+} ions and a variable amount of Gd^{3+} ions. The emission spectra of all the samples were obtained at two different excitation wavelengths, $\lambda_{ex} = 273$ nm (Fig. 4(a)) and $\lambda_{ex} = 298$ nm (Fig. 4(b)). The broad band centered around 335 nm found in all emission spectra corresponds to radiative transitions in Ce^{3+} from the lowest $5d^1$ excited state to the $4f^1$ ground state, which is split into two energy levels ($^2F_{5/2}$ and $^2F_{7/2}$) due to spin-orbital coupling. Therefore, the obtained emission bands contain two Ce^{3+} peaks, which correspond to $5d \rightarrow {}^2F_{5/2}$ and $5d \rightarrow {}^2F_{7/2}$ radiative transitions in Ce^{3+} and which are most obvious in the emission spectra of x = 0.0 at. % Gd^{3+} powder sample in Fig. 4(b). By including Gd^{3+} ions and increasing their content, a redshift of the center of the broad band could be observed in both Fig. 4(a) and (b). This shift can be attributed to the change in the crystal field environment of Ce^{3+} in the presence of large Gd^{3+} ions, which affects the *d-d* orbital splitting [34,35]. It can also be noted that the separation of the aforementioned Ce^{3+} peaks in the sample without Gd^{3+} ions is around 1400 cm^{-1}, and it increases up to 2000 cm^{-1} along with the doping level of Gd^{3+} [19,36]. Unlike Ce^{3+} ions, the host environment does not affect energy levels of Gd^{3+} ions due to their stable configuration with the half-filled $4f^7$ shell and the shielding effect of their 5s and 5p orbitals [34].

Small peak rising at around 312 nm (inset in Fig. 4(a)) upon incorporation of Gd^{3+} is a result of a creation of a narrow dip at around 313 nm, which coincides with the absorption line corresponding to spin and parity forbidden f-f optical transition ($^8S_{7/2} \rightarrow {}^6P_J$) in Gd^{3+} [37,38]. The presence of dip in the Ce^{3+} emission spectrum can be an indication of the

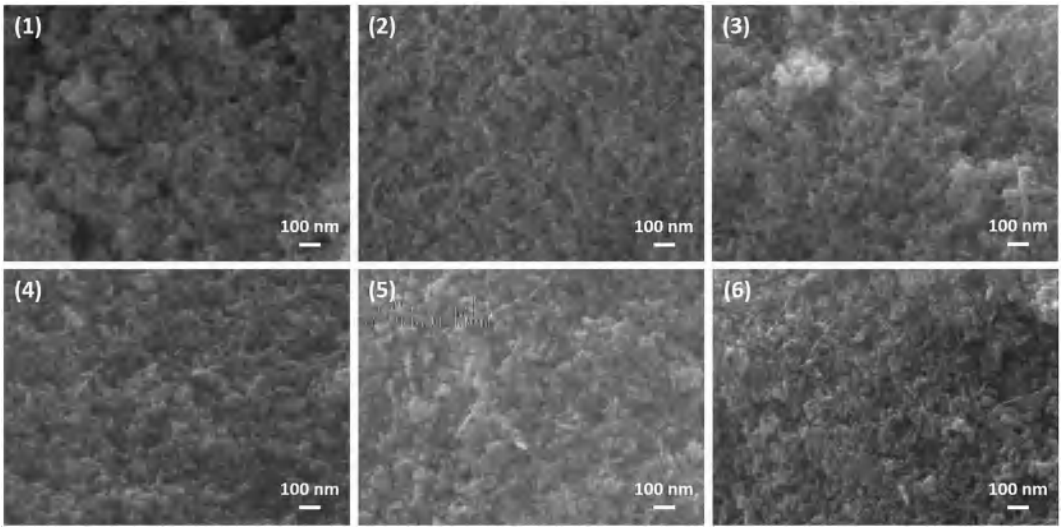

Fig. 3. FE-SEM micrographs of as-prepared (Gd, Ce): SrF_2 powder samples with 3.0 at. % Ce^{3+} and (1) 0.0, (2) 0.5, (3) 1.0, (4) 1.5, (5) 2.0, and (6) 3.0 at. % Gd^{3+}.

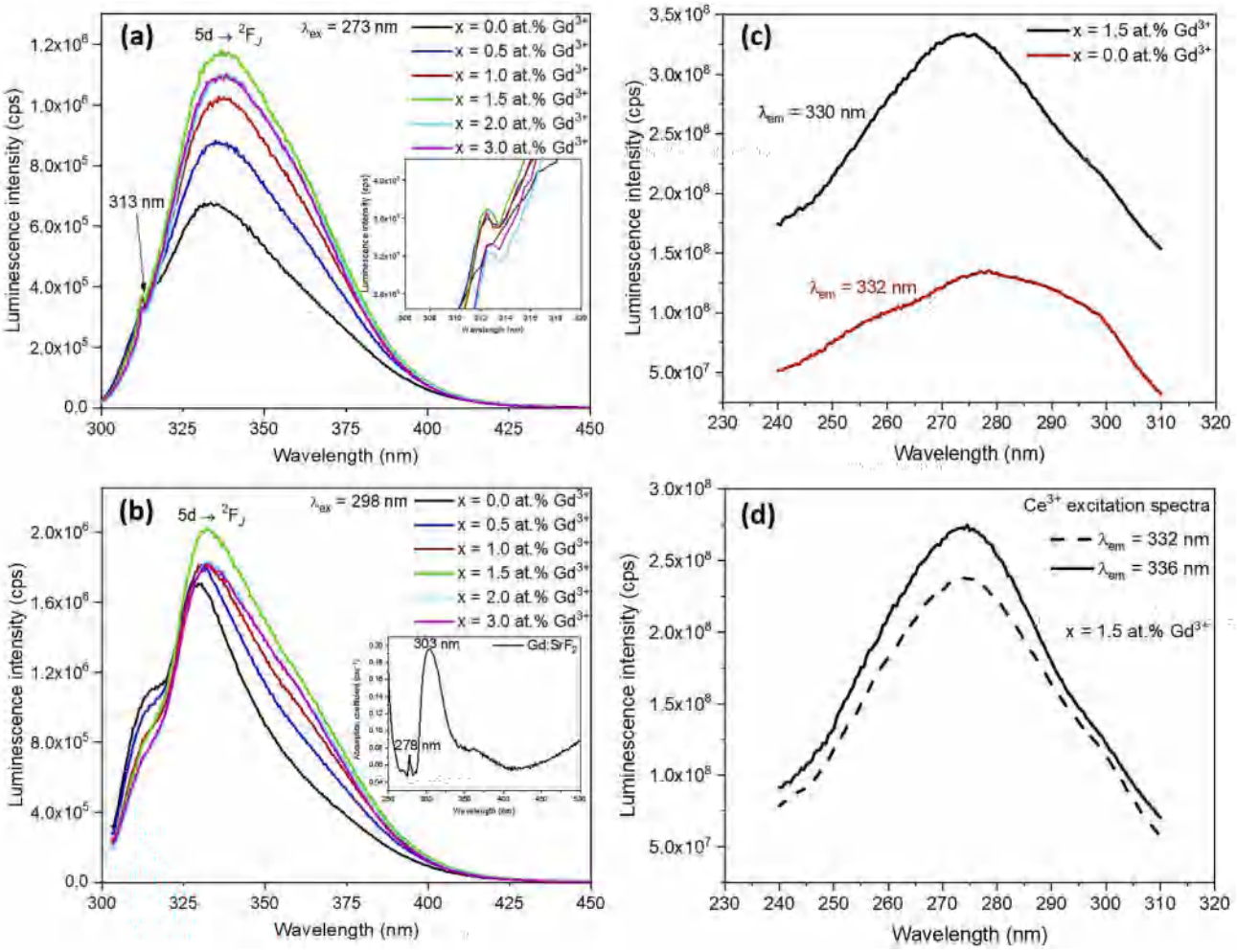

Fig. 4. PL emission spectra of as-prepared (Gd, Ce): SrF_2 powder samples under (a) $\lambda_{ex} = 273$ nm and (b) $\lambda_{ex} = 298$ nm excitation. Inset **4**(a): PL emission spectra around 313 nm dip. Inset **4**(b): Absorption spectrum of 0.5 at. % doped Gd: SrF_2 powder sample; (c) PL excitation spectra of undoped (0.0 at. % Gd^{3+}) - red line, and doped (1.5 at. % Gd^{3+}) - black line, powder samples; (d) PL excitation spectra of Ce^{3+} in 1.5 at. % Gd^{3+}-doped sample for $\lambda_{em} = 336$ nm (solid line) and $\lambda_{em} = 332$ nm (dashed line).

existence of radiative energy transfer from Ce^{3+} to Gd^{3+}, where the Gd^{3+} ions re-absorb the luminescence coming from Ce^{3+} ions. The higher the Gd^{3+} content, the larger the 313 nm dip is, and therefore, the higher the intensity of the resulting 312 nm peak. On the other hand, the increase of the intensity of the Ce^{3+} peaks around 335 nm ($5d \rightarrow {}^2F_J$) with Gd^{3+} concentration can be an effect of the change in the local symmetry of the Ce^{3+} activator ion resulting from the incorporation of extra F^- ions in the structure [39].

The emission spectra presented in Fig. 4(b) can be explained with a similar analogy to the one used in Fig. 4(a). The energy emitted from Ce^{3+} ($5d \rightarrow {}^2F_J$) upon absorption of the upcoming 298 nm excitation is re-absorbed by Gd^{3+} ions through the radiative energy transfer, but probably with much lower efficiency than the former, which could be the reason why Gd^{3+} dip is not visible in the spectra in Fig. 4(b). Direct excitation of the Gd^{3+} ions with 298 nm wavelength and, therefore, the emission is, in general, not expected at this wavelength in SrF_2 host [37, 40]. However, the absorption spectrum of the single-doped Gd: SrF_2 (0.5 at. % Gd^{3+}) powder sample presented in the inset of Fig. 4(b) demonstrates the existence of a broad band absorption centered around 303 nm, which can originate from the ${}^8S_{7/2} \rightarrow {}^6P_J$ transitions in Gd^{3+} [38]. Although the absorption around 298 nm wavelength is possible, based on the absorption spectrum of Gd^{3+}, it is very weak and inefficient, so its contribution is minor; therefore, no Gd^{3+} emission peaks can be observed in Fig. 4(b).

A change in the shape of the emission spectra with Gd^{3+} concentration could be explained with the existence of different Ce^{3+} sites [15,41], which contribute to the emission bands with a different ratio upon excitation. This would also account for some difference in the emissions excited at 273 nm (Fig. 4(a)) and at 298 nm (Fig. 4(b)). However, such an explanation would require additional measurements that are not in the scope of this paper.

It should be pointed out that the 273 nm excitation is by far more efficient for Ce^{3+} than for Gd^{3+}. This comes from the fact that the 4f-4f transitions in Gd^{3+} are forbidden while the 4f-5d transitions in Ce^{3+} are fully allowed. For such a reason, even in the sample with the highest Gd^{3+} concentration (3 at. %), Gd^{3+} cannot compete for the incoming energy with Ce^{3+} whose transitions are by far more probable.

Excitation spectra of two 3.0 at. % Ce: SrF_2 powder samples doped with 0.0 at. % Gd^{3+} (red line spectrum) and 1.5 at. % Gd^{3+} (black line spectrum) are presented in Fig. 4(c). Fig. 4(d) presents the excitation spectra of 1.5 at. % Gd^{3+} doped sample which correspond to $\lambda_{em} = 336$ nm (solid line) and $\lambda_{em} = 332$ nm (dashed line) emission peaks of Ce^{3+} ion excited with 273 nm and 298 nm light, respectively. Broad absorption bands can be a result of the crystal field splitting of 5d energy levels in Ce^{3+} [24]. It can be inferred from Fig. 4(c) that doping with Gd^{3+} ions significantly increased the efficiency of absorption (more than double), as observed elsewhere [42]. Additionally, a slight difference in shapes of the excitation spectra of Gd^{3+}-doped and undoped samples can result from the differences in crystal fields of these two samples with distinct compositions.

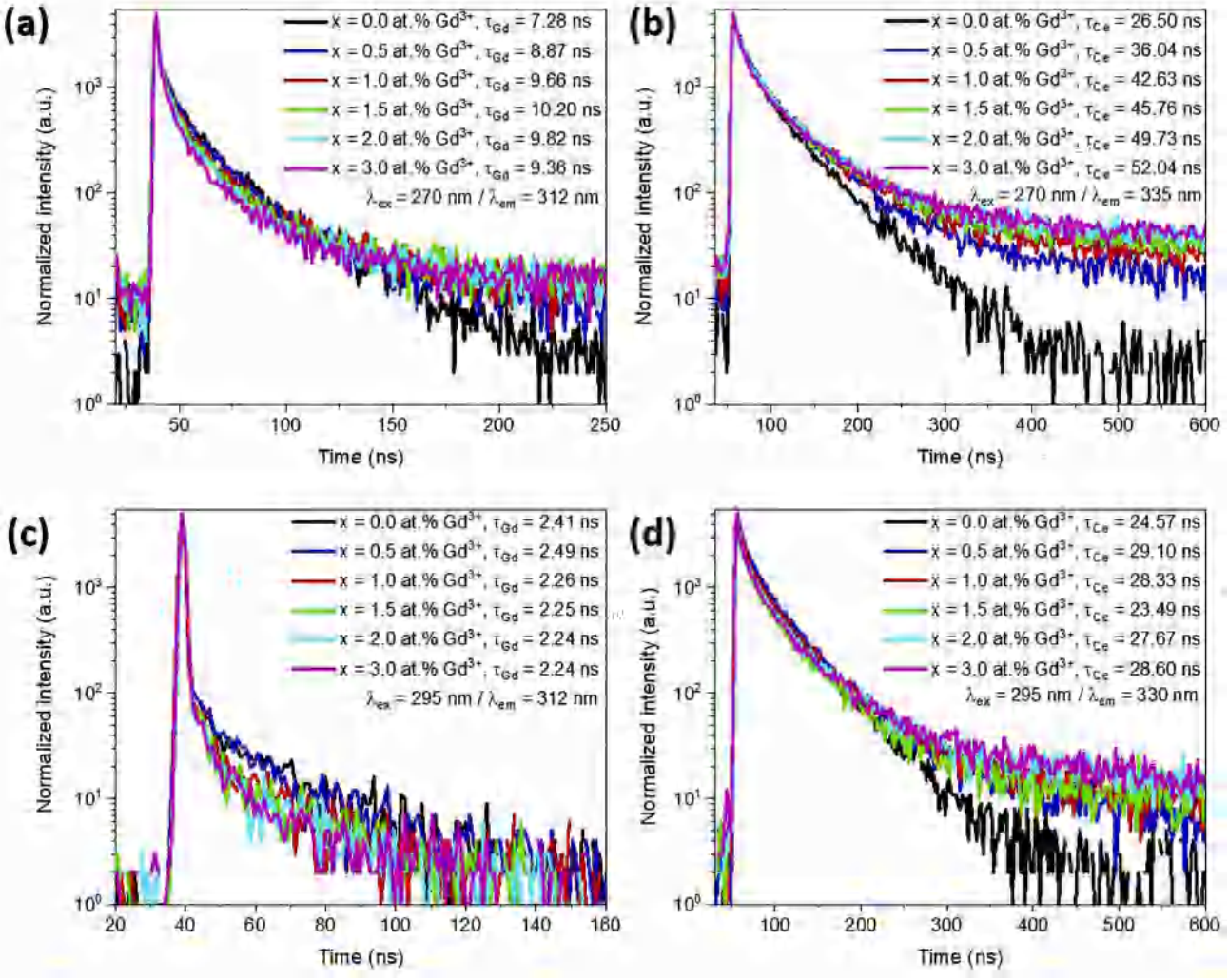

Fig. 5. PL decay curves of 3.0 at. % Ce^{3+}: Gd_xSrF_2 (x = 0.0, 0.5, 1.0, 1.5, 2.0, and 3.0 at. % Gd^{3+}) powder samples measured at RT for (a) Gd^{3+} and (b) Ce^{3+} emission excited by $\lambda_{ex} = 270$ nm, and (c) Gd^{3+} and (d) Ce^{3+} emission excited by $\lambda_{ex} = 295$ nm.

The powder samples were further examined via photoluminescence lifetime measurements by analyzing the obtained luminescence decay curves. The decay curves for Ce^{3+} ($5d \rightarrow {}^2F_J$) emission around 330 nm and Gd^{3+} (${}^6P_J \rightarrow {}^8S_{7/2}$) characteristic (expected) emission at 312 nm, excited by λ_{ex} = 295 nm and λ_{ex} = 270 nm absorption peaks, were measured at RT for the as-prepared (Gd, Ce): SrF_2 powder samples. The results of the photoluminescence lifetime measurements are presented in Fig. 5 as normalized decay curves. The average luminescence lifetime (τ) was estimated as the value proportional to the area under the decay curve [43]. Considering a much lower excitation probability of Gd^{3+} mentioned earlier, compared to Ce^{3+}, short luminescence lifetimes of the 312 nm emission upon both 270 nm and 295 nm excitations (Fig. 5 (a) and (c)) are a result of a dominant Ce^{3+} excitation. Typical Gd^{3+} decay times are found in the μs- or more often ms-range [31,44]. Very fast (<100 ns) decay times are a characteristic of Ce^{3+} ion in fluoride hosts, and the fact that these decay times remain constant with an increase of Gd^{3+} concentration in the samples, further confirms the dominant effect of Ce^{3+} ions over Gd^{3+} in (Gd, Ce): SrF_2. If the radiative energy transfer is taking place, then the Ce^{3+} decay time will remain the same; conversely, if the non-radiative energy transfer occurs, the Ce^{3+} decay time will decrease due to the transfer of energy from Ce^{3+} to Gd^{3+} [45]. This confirms the initial assumption of the radiative energy transfer from Ce^{3+} to Gd^{3+} observed in the spectra in Fig. 4. Furthermore, all the decays are non-exponential, which most probably comes from the fact that Ce^{3+} experiences some differences in the local symmetry due to the necessity to compensate its extra charge by additional F^- ions. Additionally, the small size of the crystallites makes a significant fraction of the activators experiencing all the surface-related effects, such as distortion of local symmetries, dangling bonds, adsorbed molecules of air-gasses, etc.

The average decay times of Ce^{3+} emission at 335 nm and 330 nm, upon 270 nm and 295 nm excitation, respectively, obtained from the decay curves presented in Fig. 5(b) and (d) are in the ns-range and a slight increase with an increase in Gd^{3+} concentration can be interpreted as a presence of an emission afterglow and/or a small admixture of Gd^{3+} luminescence due to the radiative energy transfer from Ce^{3+} to Gd^{3+}. The mentioned afterglow can be a result of trapped carriers (e.g. holes at Ce^{3+} and electrons at Gd^{3+}), which can be released with some delay giving rise to the delayed luminescence [46–48]. It can be concluded that the observed radiative energy transfer is a rather inefficient process. Additionally, the high content of Ce^{3+} (3 at. %) in all the samples further obscures other less efficient processes.

Fig. 6 illustrates a proposed simplified model of the energy level diagram of Ce^{3+} and Gd^{3+} in SrF_2 host material under λ_{ex} = 273 nm excitation. It is suggested that Ce^{3+} ions absorb energy in the form of a ${}^2F_J \rightarrow 5d$ optical transition (red arrow), followed by a non-radiative relaxation to the lowest 5d energy state (dashed blue arrow), and finally emission to the ground state ($5d \rightarrow {}^2F_J$) (black arrow). Only a small portion of this emission is radiatively transferred (re-absorbed) from Ce^{3+} (dashed black arrow, ET) to Gd^{3+}. Considering that the Gd^{3+} absorption under 273 nm excitation wavelength is by far less efficient than Ce^{3+}, the spin and parity forbidden 4f-4f transition (${}^8S_{7/2} \rightarrow {}^6P_J$) in Gd^{3+} was not presented in the model diagram.

3.2. (Gd, Ce): SrF_2 transparent ceramics

Applying the vacuum hot-pressing method (HP), a highly transparent (Gd, Ce): SrF_2 (1.5 at. % Gd^{3+} and 3.0 at. % Ce^{3+}) ceramics was obtained using the nanoparticle powder that showed the highest intensity of the luminescence emission. The measured relative density of the bulk ceramic sample represents 98.81% of the theoretical density. XRD measurement confirms previous results obtained for the powder samples. XRD diffractogram of the ceramic sample with cubic SrF_2 phase is presented in Fig. 1(a).

Fig. 7 shows SEM micrograph of the polished surface of the ceramic sample. No second phase could be observed from the SEM image;

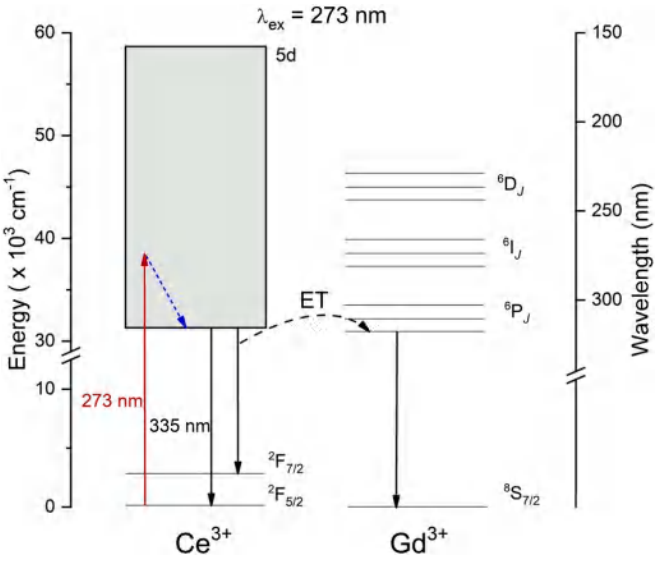

Fig. 6. Proposed model of the energy level diagrams of Gd^{3+} and Ce^{3+} under λ_{ex} = 273 nm excitation; on the diagram are presented: excitation transition (solid red line), radiative emission transition (solid black line), non-radiative relaxation (dashed blue line), and radiative energy transfer (ET) (dashed black line).

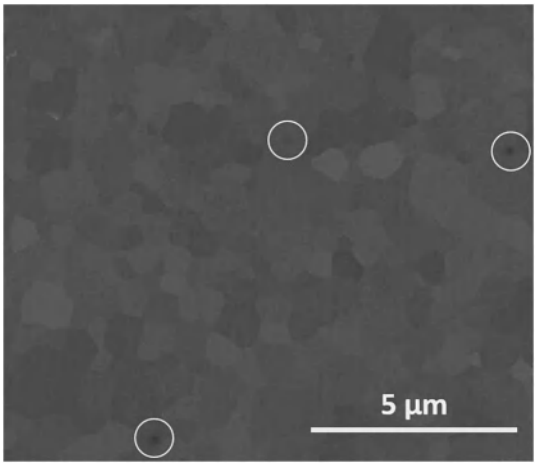

Fig. 7. SEM micrograph of the mirror-polished surface of (Gd, Ce): SrF_2 transparent ceramics. White circles point out at the residual porosity.

however, the pores, which remained entrapped in the sample during sintering, could be detected. An average grain size of 1.1 μm was calculated by applying the method of linear intercepts and using the software Nano Measurer 1.2.

In-line optical transmittance of a (Gd, Ce): SrF_2 ceramic sample was measured in the wavelength region from 200 nm to 1000 nm. Optical transmittance increases with wavelength and reaches its maximum of 75.2% at 1000 nm, as displayed in Fig. 8. A photograph of the polished (Gd, Ce): SrF_2 ceramic sample with the 10 mm diameter and 0.90 mm thickness is presented as an inset in the bottom right corner of Fig. 8. The sample appears transparent when observed by the naked eye.

Considering the above results, it can be concluded that the unsatisfactory optical quality of the (Gd, Ce): SrF_2 ceramics compared to the theoretical value calculated for the SrF_2 single crystal (93.66%) [27] is most probably due to the residual pores present in the sample. In cubic optical materials such as SrF_2, CaF_2 and YAG, the most common light scattering centers are found to be the residual pores [28]. The small

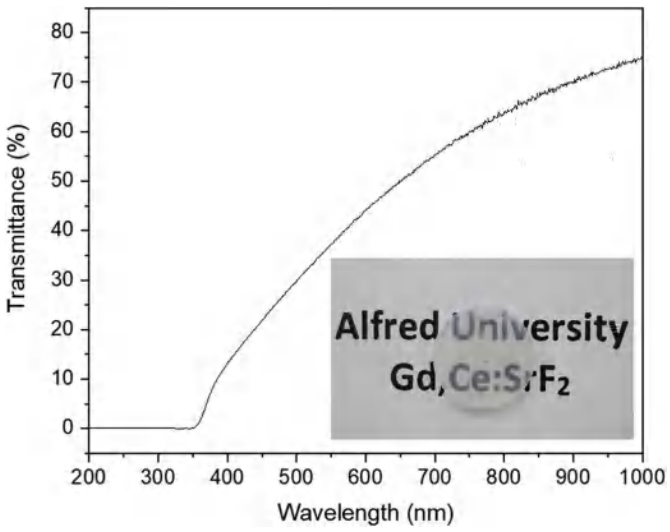

Fig. 8. In-line transmittance spectrum of (Gd, Ce): SrF_2 transparent ceramics. Inset: A photograph displaying (Gd, Ce): SrF_2 transparent ceramic sample sintered at 820 °C for 60 min under a 30 MPa loading pressure in the vacuum hot-pressing furnace.

pores become detrimental to transparency of the sintered ceramics and cause optical losses, especially in the short wavelength range. Additionally, a presence of K^+ ions in the powder sample used for fabrication of transparent ceramics, that was revealed during the EDS measurements (Fig. 2), may represent another factor which can negatively affect optical quality of the transparent ceramics [29]. Nevertheless, the highest optical transmittance achieved for (Gd, Ce): SrF_2 ceramic is the same or even higher than for other reported rare-earth doped SrF_2 transparent ceramics at the same wavelength [29,49]. In the UV range, in-line transmittance at 400 nm was measured to be 13.2% which is higher than in other reports [29]. As suggested by other authors, this value can be significantly increased by the application of monodispersed nanoparticles as a starting material or nanopowders free from agglomerations [49], or by further adjusting of the processing parameters during sintering. This work will be continued.

4. Conclusion

The (Gd, Ce): SrF_2 nanoparticle powders with 3.0 at. % Ce^{3+} and different concentrations of Gd^{3+} ions (0.0, 0.5, 1.0, 1.5, 2.0, and 3.0 at. %) were prepared by the co-precipitation method. All the powders have shown to have a single cubic SrF_2 phase. The photoluminescence excitation, emission, and lifetime measurements revealed that doping of Gd^{3+} ions into Ce: SrF_2 can affect the crystal field environment of Ce^{3+} ions due to the incorporation of extra F^- ions necessary to compensate for the extra charge. Broad band emission peaks in the UV range of spectra at around 335 nm can be assigned to the 5d → ^2F_J radiative transitions of Ce^{3+} in (Gd, Ce): SrF_2 upon 273 nm and 298 nm excitation. An increase of the luminescence intensity and excitation efficiency of Ce^{3+} ions upon the addition of Gd^{3+} ions were observed as an effect of a change in the crystal field and symmetry around Ce^{3+}. Photoluminescence measurements further revealed the existence of radiative energy transfer from Ce^{3+} to Gd^{3+} ions and showed that Ce^{3+} ions are more efficient in excitation and emission than Gd^{3+} due to existence of 4f-5d allowed optical transitions. (Gd, Ce): SrF_2 (1.5 at. % Gd^{3+} and 3.0 at. % Ce^{3+}) transparent ceramics were fabricated in a vacuum by the hot-pressing method at 820 °C for 60 min under a 30 MPa loading pressure. The highest in-line transmittance in the UV range was measured to be 13.2% at 400 nm. Considering the effect which incorporation of Gd^{3+} ions has on the UV luminescence intensity of Ce^{3+} ions in the (Gd, Ce): SrF_2 nanoparticle powder, as well as possibility of fabrication of such material as transparent ceramics, it can be concluded that (Gd, Ce): SrF_2 can be a promising candidate for optical applications in the UV region.

Declaration of competing Interest

We confirmed that the authors do not have any conflict of interests.

Acknowledgements

The authors gratefully acknowledge the NSF CAREER grant No. 1554094 for funding this research. The authors wish to thank Prof. Luiz Jacobsohn from the Department of Materials Science and Engineering at Clemson University for providing fluorescence lifetime measurements for this study.

References

[1] A. Ikesue, Y.L. Aung, Ceramic laser materials, Nat. Photon. 2 (2008) 721–727.
[2] T.T. Basiev, M.E. Doroshenko, V.A. Konyushkin, V.V. Osiko, P.P. Fedorov, V. A. Demidenko, K.V. Dukel′skii, I.A. Mironov, A.N. Smirnov, Fluoride optical nanoceramics, Russ. Chem. Bull., Int. Ed. 57 (2008), 887–886.
[3] F. Qin, Y. Zheng, Y. Yu, Z. Cheng, P.S. Tayebi, W. Cao, Z. Zhang, Ultraviolet and violet upconversion luminescence in Ho^{3+}-doped Y_2O_3 ceramic induced by 532-nm CW laser, J. Alloys Compd. 509 (2011) 1115–1118.
[4] F. Qin, Y. Zheng, Y. Yu, C. Zheng, P.S. Tayebi, Z. Zhang, W. Cao, Ultraviolet upconversion luminescence of Gd^{3+} from Ho^{3+} and Gd^{3+} codoped oxide ceramic induced by 532-nm CW laser excitation, Optic Commun. 284 (2011) 3114–3117.
[5] Y. Fujimoto, T. Yanagida, S. Wakahara, H. Yagi, T. Yanagidani, S. Kurosawa, A. Yoshikawa, Scintillation properties of Yb^{3+}-doped YAG transparent ceramics, Opt. Mater. 35 (2013) 778–781.
[6] T. Yanagida, Y. Fujimoto, H. Yagi, T. Yanagitani, Optical and scintillation properties of transparent ceramic Yb:Lu_2O_3 with different Yb concentrations, Opt. Mater. 36 (2014) 1044–1048.
[7] F. Nakamura, T. Kato, G. Okada, N. Kawaguchi, K. Fukuda, T. Yanagida, Scintillation and dosimeter properties of CaF_2 transparent ceramics doped with Nd^{3+} produced by SPS, J. Eur. Ceram. Soc. 37 (2017) 4919–4924.
[8] J. Luo, L. Ye, J. Xu, Preparation and properties of Ce^{3+}:BaF_2 transparent ceramics by vacuum sintering, J. Nanosci. Nanotechnol. 16 (2016) 3985–3989.
[9] F. Nakamura, T. Kato, G. Okada, N. Kawaguchi, K. Fukuda, T. Yanagida, Scintillation and storage luminescence properties of MgF_2 transparent ceramics doped with Ce^{3+}, Opt. Mater. 72 (2017) 470–475.
[10] P. Gredin, M. Mortier, Optical properties of fluoride transparent ceramics, in: A. Tressaud, K. Poeppelmeier (Eds.), Photonic and Electronic Properties of Fluoride Materials, Elsevier, 2016, pp. 65–87.
[11] Y. Su, M. Liu, D. Han, L. Li, T. Wang, X. Wang, Ce^{3+} and Ln^{3+} (Ln = Dy, Eu, Sm, Tb) codoped SrF_2 nanoparticles: synthesis and multicolor light emission, J. Nanosci. Nanotechnol. 16 (2016) 3956–3960.
[12] C. Zhang, Z. Hou, R. Chai, Z. Cheng, Z. Xu, C. Li, L. Huang, J. Lin, Mesoporous SrF_2 and SrF_2:Ln^{3+} (Ln = Ce, Tb, Yb, Er) hierarchical microspheres: hydrothermal synthesis, growing mechanism, and luminescent properties, J. Phys. Chem. C 114 (2010) 6928–6936.
[13] L.v. Pieterson, M.F. Reid, R.T. Wegh, S. Soverna, A. Meijerink, $4f^n$-$4f^{n-1}5d$ transitions of the light lanthanides: experiment and theory, Phys. Rev. B 65 (2002), 045113.
[14] N.M. Khaidukov, S.K. Lam, D. Lo, V.N. Makhov, Observation of Time-transient spectral narrowing at 309 nm in Ce^{3+} doped SrF_2 crystal, Optic Commun. 205 (2002) 415–420.
[15] E. Radzhabov, T. Kurobori, Cubic and tetragonal Ce^{3+} ions in strontium fluoride, Radiat. Meas. 38 (2004) 523–527.
[16] E.J. Bosze, G.A. Hirata, L.E. Shea-Rohwer, J. McKittrick, Improving the efficiency of a blue-emitting phosphor by an energy transfer from Gd^{3+} to Ce^{3+}, J. Lumin. 104 (2003) 47–54.
[17] K. Mori, M. Nakayama, Role of the core excitons formed by 4*f*-4*f* transitions of Gd^{3+} on Ce^{3+} scintillation in Gd_2SiO_5 : Ce^{3+}, Phys. Rev. B 67 (2003) 165206.
[18] J.M. Sun, S. Prucnal, W. Skorupa, M. Helm, L. Rebohle, T. Gebel, Increase of blue electroluminescence from Ce-doped SiO_2 layers through sensitization by Gd^{3+} ions, Appl. Phys. Lett. 89 (2006), 091908.
[19] J. Zhong, H. Liang, H. Lin, B. Han, Q. Su, G. Zhang, Effects of crystal structure on the luminescence properties and energy transfer between Gd^{3+} and Ce^{3+} ions in $MGd(PO_3)_4$:Ce^{3+} (M = Li, Na, K, Cs), J. Mater. Chem. 17 (2007) 4679–4684.
[20] G. Stryganyuk, T. Shalapska, A. Voloshinovskii, A. Gektin, A. Krasnikov, S. Zazubovich, Processes of the excitation energy migration and transfer in Ce^{3+}-doped alkali gadolinium phosphates studied with time-resolved photoluminescence spectroscopy technique, J. Lumin. 131 (2011) 2027–2035.
[21] V. Schiopu, A. Matei, A. Dinescu, M. Danila, I. Cernica, Ce, Gd codoped YAG nanopowder for white light emitting device, J. Nanosci. Nanotechnol. 12 (2012) 8836–8840.

[22] P. Demchenko, A. Gektin, A. Krasnikov, I. Pashuk, T. Shalapska, G. Stryganyuk, A. Voloshinovskii, S. Zazubovich, Energy migration and $Gd^{3+} \leftrightarrow Ce^{3+}$ transfer in Ce^{3+}-doped GdP_3O_9 metaphosphate, J. Phys. D Appl. Phys. 46 (2013) 235103.
[23] Z. Onderisinova, M. Kucera, M. Hanus, M. Nikl, Temperature-dependent nonradiative energy transfer from Gd^{3+} to Ce^{3+} ions in co-doped LuAG:Ce,Gd garnet scintillators, J. Lumin. 167 (2015) 106–113.
[24] S. Jang, J. Lim, Y.S. Lee, Study on the emission property of YBO_3 with Co-doping of Ce and Gd ions, J. Kor. Phys. Soc. 71 (2017) 166–170.
[25] G.K. Miner, T.P. Graham, G.T. Johnston, Effect of a Ce^{3+} codopant on the Gd^{3+} EPR spectrum of SrF_2 at room temperature, J. Chem. Phys. 57 (1972) 1263–1270.
[26] T. Sizova, E. Radzhabov, Photochromism in calcium and strontium fluoride crystals doped with rare-earths ions, IEEE Trans. Nucl. Sci. 59 (2012) 2098–2101.
[27] W. Li, B. Mei, J. Song, Z. Wang, Fabrication and optical property of highly transparent SrF_2 ceramic, Mater. Lett. 159 (2015) 210–212.
[28] Z. Liu, B. Mei, J. Song, D. Yuan, Z. Wang, Microstructure and optical properties of hot-pressed Er:CaF_2 transparent ceramics, J. Alloys Compd. 646 (2015) 760–765.
[29] W. Li, H. Huang, B. Mei, J. Song, Synthesis of highly sinterable Yb: SrF_2 nanopowders for transparent ceramics, Opt. Mater. 75 (2018) 7–12.
[30] M.I. Mendelson, Average grain size in polycrystalline ceramics, J. Am. Ceram. Soc. 52 (1969) 443–446.
[31] G. Yi, W. Li, J. Song, B. Mei, Z. Zhou, L. Su, The effect of Gd^{3+} ions on fabrication and luminescence properties of Nd^{3+}-doped $(Ca_{1-x}Gd_x)F_{2+x}$ transparent ceramics, Mater. Res. Bull. 102 (2018) 304–310.
[32] X. Xie, B. Mei, J. Song, W. Li, L. Su, Fabrication and spectral properties of Nd, La: CaF_2 transparent ceramics, Opt. Mater. 76 (2018) 111–116.
[33] W. Li, B. Mei, J. Song, W. Zhu, G. Yi, Yb^{3+} doped CaF_2 transparent ceramics by spark plasma sintering, J. Alloys Compd. 660 (2016) 370–374.
[34] H. Shi, C. Zhu, J. Huang, J. Chen, D. Chen, W. Wang, F. Wang, Y. Cao, X. Yuan, Luminescence properties of YAG:Ce, Gd phosphors synthesized under vacuum condition and their white LED performances, Opt. Mater. Express 4 (2014) 649–655.
[35] M. Kucera, M. Hanus, Z. Onderisinova, P. Prusa, A. Beitlerova, M. Nikl, Energy transfer and scintillation properties of Ce^{3+} doped $(LuYGd)_3(AlGa)_5O_{12}$ multicomponent garnets, IEEE Trans. Nucl. Sci. 61 (2014) 282–289.
[36] E. Radzhabov, Charge transfer luminescence in Ce-doped fluorides, Radiat. Eff. Defect Solid 158 (2003) 203–207.
[37] J. Makovsky, Optical spectra of Gd^{3+} in SrF_2 and BaF_2, J. Chem. Phys. 46 (1967) 390–391.
[38] F. Zhang, X. Fan, J. Liu, F. Ma, D. Jiang, S. Pang, L. Su, J. Xu, Dual-wavelength mode-locked operation on a novel Nd^{3+},Gd^{3+}:SrF_2 crystal laser, Opt. Mater. Express 6 (2016) 1513–1519.
[39] S.S. Pote, C.P. Joshi, S.V. Moharil, P.L. Muthal, S.M. Dhopte, Luminescence of Ce^{3+} in $Ca_{0.65}La_{0.35}F_{2.35}$ host, J. Lumin. 130 (2010) 666–668.
[40] P.P. Yaney, J.A. Detrio, J.M. O'Hare, C.W. Searle, R.L. Jones, Research and Development on Laser, Semiconducting and Magnetic Materials, Technical Report: AFML-TR-73-52, Air Force Materials Laboratory, Dayton, OH, 1973.
[41] V.N. Makhov, S.K. Batygov, L.N. Dmitruk, M. Kirm, S. Vielhauer, G. Stryganyuk, VUV 5*d*-4*f* luminescence of Gd^{3+} and Lu^{3+} ions in the CaF_2 host, Phys. Solid State 50 (2008) 1625–1630.
[42] F. Huang, L. Dong, Z. Fu, H. Wang, W. Wang, Y. Wang, Study of co-excited green emission of Tb^{3+}, Ce^{3+} and Gd^{3+} in yttrium aluminum garnet, J. Ceram. Process. Res. 10 (2009) 807–811.
[43] J.R. Lakowicz, Principles of Fluorescence Spectroscopy, third ed., Springer US, 2006.
[44] M. Kucera, M. Nikl, M. Hanus, Z. Onderisinova, Gd^{3+} to Ce^{3+} energy transfer in multi-component GdLuAG and GdYAG garnet scintillators, Phys. Status Solidi RRL 7 (2013) 571–574.
[45] Q. Zhang, H. Ni, L. Wang, F. Xiao, Luminescence properties and energy transfer of $GdAl_3(BO_3)_4$:Ce^{3+}, Tb^{3+} phosphor, Ceram. Int. 42 (2016) 6115–6120.
[46] H. Wu, C. Yang, Z. Zhang, Y. Tang, Photoluminescence and thermoluminescence of Ce^{3+} incorporated $Y_3Al_5O_{12}$ synthesized by rapid combustion, Optik 127 (2016) 1368–1371.
[47] H. Luo, A.J.J. Bos, P. Dorenbos, Controlled electron-hole trapping and detrapping process in $GdAlO_3$ by valence band engineering, J. Phys. Chem. C 120 (2016) 5916–5925.
[48] H. Guo, Y. Wang, W. Chen, W. Zeng, G. Li, Y. Li, $Ca_6BaP_4O_{17}$:Eu^{2+},Gd^{3+}: a yellow emitting long lasting phosphor with high brightness and long afterglow duration, New J. Chem. 40 (2016) 613–618.
[49] J. Liu, P. Liu, J. Wang, X. Xu, D. Li, J. Zhang, X. Nie, Fabrication and sintering behavior of Er:SrF_2 transparent ceramics using chemically derived powder, Mater. Lett. 11 (2018) 475.